ISIMA 2011 Project

Convectively Generated Zonal Jets by Thunderstorms on Jupiter

Xi Zhang[1] and Adam Showman[2]

[1]Division of Geological and Planetary Sciences, California Institute of Technology, Pasadena, CA, 91125, USA, xiz@gps.caltech.edu

[2]Department of Planetary Sciences, Lunar and Planetary Laboratory, University of Arizona, Tucson, AZ, 85721, USA

1. ABSTRACT

A forced-dissipative shallow water model is adopted to simulate the jet streams, especially the equatorial flow, on Jupiter. Two types of forcing, the local mass pulse and vorticity pulse, are used to parameterize the small scale moist convection such as thunderstorms, respectively. In the mass-forced dissipative model without the frictional drag, it is unable to produce a prograde flow at equator. The reason could be that the anticyclonic features are favored by the off-equator positive mass forcing. In the simulations with the vorticity-type forcing, equatorial superrotation could be produced under some condition, although the physical mechanism is not fully understood.

2. INTRODUCTION

Since the Voyager era, about a dozen stable zonal jets have been observed on the boundaries of the dark belts and bright zones in each hemisphere of Jupiter. The wind direction of jet stream is alternating with latitude and therefore results in cyclonic shear in the belts and anticyclonic shear in zones (Vasavada and Showman, 2005). Previous studies suggested that small-scale eddies accelerate the jets by transferring eastward momentum into the prograde (eastward) jets and westward momentum into the retrograde (westward) jets (so-called 'inverse energy cascade process') (Ingersoll et al., 1981; Salyk et al, 2006). However, the source of eddies, especially, the mechanism that produces a broad, strong, prograde equatorial flow with a peak velocity of ~ 150 m s^{-1} (so-called 'superrotation'), remains unsolved. It was proposed that small-scale turbulences generated from the deep cloud layer by moist convection, such as thunderstorms, might be the candidate (Gierasch et al, 2000; Ingersoll et al., 2000). A two dimensional quasigeostrophic model forced by moist convection (Li et al., 2006) successfully produced multiple jet streams for Jupiter and Saturn. However, quasigeostrophic approximation is not proper for the equatorial region. A thunderstorm-forced-dissipative shallow-water model by Showman (2007) generated multiple jets in Jupiter's atmosphere, but only westward jets at equator. Recently, Lian and Showman (2010) used a 3-D general circulation model and found that the large-scale latent heat released associated with moist convection produces multiple jet streams in gas giant planets regime. Moreover, their simulations produce prograde equatorial jets on Jupiter and Saturn and retrograde jets on Uranus and Neptune, qualitatively consistent with the observations. Alternatively, Schneider and Liu (2009) and Liu and Schneider (2010) proposed that the prograde equatorial jets could result from the convective Rossby waves generated from the internal heat trapped in the deep interiors of giant planets during the planetary formation period. Their simulations with a dry convective scheme also produced the jet patterns

consistent with the observations.

The three dimensional general circulation model is the most complete weather model for the atmospheric dynamics study. However, the model is too complicated to analyze the basic physical mechanisms. Instead, we adopt a simpler shallow-water model in this study and ask the following basic questions: is a shallow water model able to produce prograde jet streams in the equatorial region? If yes, under what condition? If no, why?

Shallow-water system is the simplest dynamic system allowing large-amplitude column stretching (Showman, 2007), but the whole system is still barotropic, i.e., no column twisting or tilting. The freely-evolving shallow water model (e.g., Cho and Polvani,1996) and freely-decaying model (e.g., Iacono et al., 1999) with vortex patches in the beginning, seem not be able to generate prograde jets at equator. In the forced-dissipative shallow water simulations, Showman (2007) parameterized the latent heat release by the thunderstorm forcing as adding mass into the weather layer, but only retrograde equatorial jets (subrotation) was obtained. By applying the vorticity-type turbulence forcing, and the dissipation due to radiative relaxation and frictional drag, Scott and Pavolni (2007) obtained the similar results as Showman (2007). They pointed that the large-scale energy dissipation is crucial in determining the direction of equatorial jets. On the other hand, Scott and Polvani (2008) successfully generated the superrotation under vorticity forcing without linear frictional drag, and the authors attributed the reason to the radiative relaxation which would damp anticyclones at a faster rate than cyclones, although the physical mechanism was not clearly explained. Therefore, we focus on the forced-dissipative shallow water simulations in this study. Particularly, a thunderstorm-type forcing, both in mass and vorticity form, will be considered.

3. MODEL DESCRIPTION

Our shallow water model is a 'one and a half' layer model, with a steady abyssal layer beneath to represent the stable deep convective interior, and a barotropic, buoyant upper layer with uniform density to represent the upper troposphere of Jupiter. Thunderstorm forcing is applied to the upper layer. There are two ways to parameterize this effect in the shallow water system. A Local mass forcing applied to the layer thickness represents the isobar lifting due to the latent heat release from moist convection. On the other hand, the mass ejected into the weather layer usually produces anticyclonic vorticity in the mid-latitude, therefore the moist convection could also be parameterized as a local vorticity pulse in the system. Both of the two types of forcing are considered in this study. Radiation cooling and frictional drag are the main dissipative processes. If there is a continuous forcing, one can expect the system will reach a long-term steady state when the dissipation and forcing are balanced with each other.

In a mass forced-dissipative system, in terms of horizontal velocity $\mathbf{u}$ and upper layer geopotential $\phi = gh$, where g is gravity and h is layer thickness, the governing equations are (Vallis, 2006):

$$\frac{d\mathbf{u}}{dt} + \nabla\phi + f\mathbf{k} \times \mathbf{u} = \mathbf{R} - \frac{\mathbf{u}}{\tau_{drag}} \quad [1]$$

$$\frac{d\phi}{dt} + \nabla \cdot (\mathbf{u}\phi) = \mathbf{Q}_{rad} + \mathbf{F}_h \quad [2]$$

where $d/dt = \partial/\partial t + \mathbf{u} \cdot \nabla$ is the material derivative, $\mathbf{k}$ is the upward unit vector, τ_{drag} is frictional dissipation timescale, $f = 2\Omega\sin\theta$ is Coriolis parameter, Ω is planetary rotation rate, and θ is latitude. $\mathbf{Q}_{rad}$ is the radiative dissipation term and will be explained later. $\mathbf{F}_h$ is the mass forcing term applied to the layer thickness. $\mathbf{R}$ is the advective drag term suggested by Showman and Polvani (2010) to represent the momentum exchange

between the upper and lower layers.

In a vorticity forced-dissipative system, the equations, in terms of vorticity $\zeta = \nabla \times \mathbf{u}$, divergence $\delta = \nabla \cdot \mathbf{u}$, and geopotential ϕ, are:

$$\frac{d\zeta}{dt} + \nabla \cdot (\mathbf{u}\zeta_a) = -\frac{\zeta}{\tau_{drag}} + \mathbf{F}_\zeta \quad [3]$$

$$\frac{d\delta}{dt} - \mathbf{k} \cdot \nabla \times (\mathbf{u}\zeta_a) = -\nabla^2(\frac{|\mathbf{u}|^2}{2} + \phi) - \frac{\delta}{\tau_{drag}} \quad [4]$$

$$\frac{d\phi}{dt} + \nabla \cdot (\mathbf{u}\phi) = \mathbf{Q}_{rad} \quad [5]$$

where $\zeta_a = \zeta + f$ is the absolute vorticity. $\mathbf{F}_\zeta$ is the vorticity forcing term.

In this study, we adopt the NCAR Spectral Transform Shallow Water Model (STSWM, Hack and Jakob, 1992), which solves shallow-water equations using spectral transfer method in spherical geometry.

Same as Showman (2007), the radiative damping term $\mathbf{Q}_{rad}$ is expressed as a mass sink which is composed of two parts:

$$\mathbf{Q}_{rad} = -\frac{< \phi > -\phi_{eq}}{\tau_{mass}} - \frac{\phi - < \phi >}{\tau_{APE}} \quad [6]$$

where ϕ_{eq} is a equilibrium geopotential associated with the deformation radius $L_d = \sqrt{\phi_{eq}}/2\Omega$. $< \phi >$ is the current global averaged geopotential. τ_{mass} and τ_{APE} are the timescales to remove the mean layer mass and available potential energy, respectively. In order to be consistent with the observed deformation radius of the Great Red Spot ($L_d \sim 1000$ km, Cho et al. 2001) and Jupiter's rotation rate $\Omega = 1.74 \times 10^4$ s^{-1}, we choose $\phi_{eq} = 10^5$ m^2 s^{-1}. The relaxation timescale $\tau_{APE} = 100$ Earth day, shorter than

the radiative timescale at 1 bar level (∼tens of Earth years) is chosen to allow for the model to compete in reasonable time. τ_{mass} is set to be 0.01 Earth day.

The thunderstorms forcing terms, $\mathbf{F}_h$ and $\mathbf{F}_\zeta$, represent the small-scale convective processes from the abyssal layer to the upper weather layer. Each storm is parameterized as a local mass or vorticity pulse with a circular gaussian shape in spacial and temporal domains (Showman, 2007). The forcing term (ejection rate) is expressed as:

$$\mathbf{F}(\mathbf{r}) = \mathbf{F}_{max}\exp[-\frac{|\mathbf{r}-\mathbf{r}_0|^2}{r_{storm}^2} - \frac{(t-t_0)^2}{\tau_{storm}^2}] \quad [7]$$

where $\mathbf{F}_{max}$ is the maximum ejection rate of mass or vorticity at the storm center $\mathbf{r}_0$, occurring at time t_0, r_{storm} is the storm radius, $|\mathbf{r}-\mathbf{r}_0|$ is the distance from the storm center to any given point $\mathbf{r}$ on the sphere, τ_{storm} is the storm lifetime. In our simulations, thunderstorm are randomly generated in space and time, with a mean time interval of 10^5 s. Storm lifetime is assumed to be constant, $\tau_{storm} = 10^5$ s. The maximum ejection rate and storm size are also randomly selected for each storm in the multiple storm cases.

In the current study, we adopt a spectral resolution of T170 (512×256), corresponding to about 0.7° per grid point. A ∇^6 hyperviscosity is used to maintain the numerical stability. By far no frictional drag is included but will be investigated in the future. For each forcing, first we carry out one-storm simulations to investigate the system behavior, and the full simulations with multiple randomly generated thunderstorms in the entire globe.

4. SIMULATION RESULTS

4.1. Mass Forcing

One-storm Case

If the system is forced by one thunderstorm at equator, superrotation occurs. Figure 1 shows the simulation results after 200 hours. Storm radius $r_{storm} = 5^\circ$ and $\mathbf{F}_{max} = 1\ \mathrm{m}^2\ \mathrm{s}^{-3}$. A Rossby wave pattern off the equator and a Kelvin wave pattern at equator are produced (see the geopotential map, upper left panel). A prograde equatorial flow is generated (upper right panel), along with two stronger eastward jets at about 5°N and 5°S. In fact, the one storm case can be analogous to the exoplanet ('Hot Jupiter') simulations as shown in Showman and Polvani (2011) if we add the other mass sink forcing on the opposite side of the globe. The mechanism of generating superrotation is essentially the same. The Northwest/Southeast titling in the Northern hemisphere and Southwest/Northeast titling in the Southern hemisphere of the velocity structures, which can be seen from the geopotential map as the velocity vectors are approximated parallel to the height field contours, generated by the Rossby and Kelvin waves are necessary for the eastward acceleration of equatorial jets (Held, 2000; Showman and Polvani, 2011). The eddy momentum flux, $u'v'$, where u' and v' denote the deviations of the zonal and meridional winds from their zonally averaged values, respectively, would lead to a convergence in the equatorial region and accelerate the zonal jets until the forcing vanishes. In the absence of damping, the relationship between the acceleration and the meridional gradient of eddy momentum flux is described as (Held, 2000):

$$\frac{\partial \bar{u}}{\partial t} = -\frac{\partial(\overline{u'v'})}{\partial y} \qquad [8]$$

The $\overline{u'v'}$ is the zonally averaged eddy momentum flux and shown in the middle right

panel of Fig 1. A negative $\overline{u'v'}$ in the north region and a positive $\overline{u'v'}$ in the south region of the equator are pumping the eddy energy into central jets. The right hand side of equation [8] is equal to the eddy flux of vorticity by definition:

$$-\frac{\partial(\overline{u'v'})}{\partial y} = \overline{\zeta' v'} \qquad [9]$$

which is shown in the lower panel. After 200 hours, when the storm forcing nearly vanishes, the system has almost no acceleration right at equator but still accelerates the equatorward edges and decelerates the poleward edges of the off equator jets, leading to a jet strength decrease and width shrinking.

In the case with one storm forcing at 10°N (Figure 2, upper panel), compared with the previous case, the potential map and zonal-mean zonal wind pattern are not symmetric about equator. The Rossby waves and kelvin waves are also generated but only a strong westward jets are formed at about 5 degree north, along with one weak eastward flow on each side. From the geopotential map we can see the Rossby wave pattern has a Southwest/Northeast pattern in the northern hemisphere, which would result in a westward eddy momentum transport into the jets. The bottom panel of Figure 2 shows the case with a storm located at 30°N. It maintains the vortex structure tilting Southwest/Northeast and only produces a eastward wind on the north side and a westward wind on the south side. The wind pattern looks more like a wind shear pattern resulting from the geopotential gradient forcing and then modulated by the Coriolis force. The reason why the vortex maintains its structure rather than merges into the zonal jets by generating Rossby waves is that the β effect is suppressed in the finite deformation radius situation (see Showman (2007) for detailed analysis).

Any geopotential anomaly off the equator tends to produces a wind shear pattern. As

shown in Figure 2, in the northern hemisphere, a eastward/westward flow will be generated on the north/south side of a geopotential anomaly because of the pressure gradient and Coriolis effect. However, if the anomaly is located at the equator, it will produce eastward flows off the equator on both hemispheres because the Coriolis parameter changes sign across the equator. The off-equatorial part of the geopotential anomaly field tends to have a westward phase shift due to the Rossby waves. In the meanwhile, the Kelvin waves, which is trapped in the equator region with a eastward group propagation, result in a eastward tilting of equatorial part of the geopotential field. The wind velocity pattern associated with this tilting type would pump the eddy momentum into the equatorial jets and lead to superrotation.

Multi-storm Case

In the multi-storm cases, we generated the storms with random forcing strength ($\mathbf{F}_{max} = 0.05-1.0$ m^2 s^{-3}) and random size ($r_{storm} = 2^\circ - 4^\circ$). The storm locations are randomly chosen between 50°S-50°N, and the average number of storms per unit area of the globe is independent of latitude. Each case is simulated for more than 2×10^4 hours to make sure the whole system has reached the steady state. We are using the proxies of total available potential energy (APE) and total kinetic energy (KE) (Figure 3, upper panel). After 2×10^4 hours, the APE is about two orders of magnitude larger than the KE. Jets are dominant in low latitude and vortices are dominant in the mid-latitude in the geopotential map, for the reason that we explained in the one-storm case. Only one strong westward equatorial jet is formed, with $\bar{u}$ about 45 m s^{-1}. This result is consistent with Showman (2007). We attribute the reason to that there are more storms occurring off the equator than those at equator. As shown in the one-storm case, off-equator storm forcing tends to provide a westward acceleration on the eqautorward side of the storm forcing. Therefore, westward acceleration would dominate the system and retrograde

equatorial jet should be expected.

Observations show that the thunderstorms only occurs in the belts other than zones. Figure 4 shows a case with the storms concentrated in the belts. In each hemisphere, we have 3 belts: $10^\circ - 20^\circ$, $30^\circ - 40^\circ$, and $50^\circ - 60^\circ$. The storm size and strength are chosen in the same way as the case in Figure 3. Multiple jets are generated but the wind shear pattern is completely opposite to the observations. For example, the simulations generate anticyclonic wind pattern in the belts where the storms are. This is consistent with the geostrophic wind balance but disagrees with the measurements. Ingersoll et al. (2000) hypothesized that in the belt region, there is an upward flow from the cloud base and a downward flow from the cloud top. Our 1.5 layer shallow water model is not able to simulate that situation.

Again, the 'multi-belt' case produces westward flow along the equator. If all the storms only occur in the equatorial region, as shown the bottom panel of Figure 4, the continuous generated equatorial Rossby and Kelvin waves help accelerate the prograde flow at equator, but that system is not able to maintain a large-amplitude jet as that observed on Jupiter unless the strength and frequency of the storm forcing are significantly enhanced. The off-equator jets are strong and reach about 100 m s^{-1} in this simulation.

4.2. Vorticity Forcing

One-storm Case

The vorticity forcing amplitude $\mathbf{F}_{max}$ is taken as 2×10^{-9} s^{-2}, which is consistent with the estimated magnitude from Li et al. (2006) based on the radiation vorticity source and fractional area of moist convection on Jupiter. Storm radius $r_{storm} = 5^\circ$. Figure 5

shows two cases with a positive vorticity source (upper panel) and a negative vorticity source (lower panel) at the equator, respectively. The positive vorticity is cyclonic in the northern hemisphere and anticyclonic in the southern hemisphere, therefore generates westward flow associated with a positive geopotential anomaly in the northern hemisphere, and a eastward flow associated with a negative geopotential anomaly in the southern hemisphere. If we move the positive vorticity source northward, say, 30°N, it will generate a prograde equatorial flow (upper panel of the Figure 6) with a cyclonic wind shear and thinner layer at its current location. On the other hand, a negative (anticyclonic) vorticity source at 30°N will produce a retrograde equatorial flow (lower panel of the Figure 6) with an anticyclonic wind shear and thicker layer at its current location. Although the positive vorticity from a cyclonic source is consistent with a prograde equatorial flow (positive vorticity) based on the Stokes theorem (vorticity conservation law), how does the vorticity propagate from 30°N to equator and why is the flow confined within the equatorial band has yet to be understood. Further study is needed.

As discussed in the one-storm mass forcing section, a positive mass anomaly would induce an anticyclonic shear, consistent with the fact that up to 90% of vortices are anticyclones on Jupiter (Mac Low and Ingersoll, 1986). However, as shown by Figure 6, an anticyclonic vorticity forcing will generate an additional strong westward flow at equator, suggesting some basic difference between the two kinds of parameterizations of moist convection.

Multi-storm Case

Since the one-storm cases are not fully understood, the behavior of the multi-storm forcing system is even beyond any discussion here. Figure 7 shows an example of two simulations with the SAME parameters. We randomly chose the storm location, forcing

amplitude ($\mathbf{F}_{max} = 0.5 - 1.0\ \mathrm{s}^{-2}$), storm size ($r_{storm} = 2^\circ - 4^\circ$), and the sign of the vorticity so that the positive and negative forcing have the equal probability. The only difference of two simulations are the random number sequence. However, one case (upper panel) generates the prograde flow at equator and the other (lower panel) produces the retrograde flow, with the comparable peak velocity of the zonal-mean zonal wind. Scott and Polvani (2008) first observed that the vorticity forcing would lead to equatorial superrotation, provided large-scale radiative relaxation. We found in this study that the vorticity forcing could also result in subrotation at equator, under the same condition. This might suggest the random vorticity forcing shallow water system has an unpredictable behavior.

5. CONCLUSIONS AND DISCUSSION

Multiple zonal jets is one of dominant weather patterns on Jupiter's fluid envelope. The equatorial superrotation on Jupiter and Saturn, along with the subrotation on Uranus and Neptune, provides a great challenge to our understanding of equatorial fluid dynamics. A unified theory might exist to explain these phenomenon. Recent three dimensional simulations have successfully captured the basic features of observations. But a simple forced-dissipative shallow water model would help uncover the essential physics. From our simulation results, we conclude that a mass-forced dissipative model without the frictional drag is unable to produce a prograde flow at equator. The reason could be that the anticyclonic features are favored by the off-equator positive mass forcing. In the simulations with the vorticity-type parameterization of moist convection, equatorial superrotation could be produced under some condition. However, more future investigations are required to understand the mechanism. And more work needs to be done for the system with a frictional drag.

Finally, one should note that there are two different views of the jets formation on Jupiter: 'Shallow-forcing scenario' and 'deep-forcing scenario'. Both the shallow-water model used in this study and the three dimensional simulations mentioned above, belong to the former, which assumes the jet streams are the weather pattern confined in the outer skin (cloud layer) of Jupiter. The deep-forcing hypothesis suggests that the jets could extend to Jupiter's deep interior such as metallic hydrogen envelope. By far it is hardly to exclude any scenario based on the current measurements. But future observations, such as JUNO mission, would help to distinguish the two mechanisms.

6. ACKNOWLEDGEMENTS

The authors thank the organizers of the 2011 ISIMA held in Peking University for providing this great opportunity of collaborative research.

REFERENCES

Cho, J. Y.-K., and L. M. Polvani (1996), The morphogenesis of bands and zonal winds in the atmospheres on the giant outer planets, *Science, 273*, 335-337.

Cho, J. Y.-K., M. de la Torre Jurez, A. P. Ingersoll, and D. G. Dritschel (2001), A high-resolution, three-dimensional model of Jupiters great red spot, *J. Geophys. Res., 106*, 5099-5105.

Gierasch, P. J., and Coauthors (2000), Observation of moist convection in Jupiters at-

mosphere, *Nature, 403*, 628-630.

Hack, J. J., and R. Jakob (1992), Description of a global shallow water model based on the spectral transform method, *NCAR Tech. Rep. NCAR/TN?343+STR*, Natl. Cent. for Atmos. Res., Boulder, Colo.

Held, I. M. (2000), Paper presented at 2000 Woods Hole Oceanographic Institute Geophysical Fluid Dynamics Program, *Woods Hole Oceanographic Institute, Woods Hole, MA* (available at http://www.whoi.edu/page.do?pid=13076).

Iacono, R., M. V. Struglia, and C. Ronchi (1999), Spontaneous formation of equatorial jets in freely decaying shallow water turbulence, *Phys. Fluids, 11*, 1272-1274.

Ingersoll, A. P., R. F. Beebe, J. L. Mitchell, G. W. Garneau, G. M. Yagi, and J.-P. Muller (1981), Interaction of eddies and mean zonal flow on Jupiter as inferred from Voyager 1 and 2 images, *J. Geophys. Res., 86*, 8733-8743.

Ingersoll, A. P., P. J. Gierasch, D. Banfield, and A. R. Vasavada, and A3 Galileo Imaging Team (2000), Moist convection as an energy source for the large-scale motions in Jupiters atmosphere, *Nature, 403*, 630-632.

Li, L., A. P. Ingersoll,and X. Huang (2006), Interaction of moist convection with zonal jets on Jupiter and Saturn, *Icarus, 180*, 113-123.

Lian, Y., and A. P. Showman (2010), Generation of equatorial jets by large-scale latent heating on giant planets, *Icarus, 207*, 373-393.

Liu, J., and T. Schneider (2010),Mechanisms of Jet Formation on the Giant Planets, *J. Atmos. Sci., 67*, 3652-3672.

Schneider, T., and J. Liu (2009), Formation of jets and equatorial superrotation on Jupiter, *J. Atmos. Sci., 66*, 579-601.

Scott, R. K., and L. M. Polvani (2007), Forced-dissipative shallow-water turbulence on the sphere and the atmospheric circulation of the gas planets, *J. Atmos. Sci, 64*, 3158-3176.

Showman, A. P. (2007), Numerical simulations of forced shallow-water turbulence: Effects of moist convection on the large-scale circulation of Jupiter and Saturn, *J. Atmos. Sci., 64*, 3132-3157.

Showman, A. P., and L. M. Polvani (2010) The Matsuno-Gill model and equatorial superrotation, *Geophys. Res. Lett. 37*, L18811, doi:10.1029/2010GL044343.

Showman, A. P., and L. M. Polvani (2011) Equatorial superrotation on tidally locked exoplanets, *Astrophys. J., 738*, 71, doi: 10.1088/0004-637X/738/1/71.

Vallis, G. K. (2006), Atmospheric and Oceanic Fluid Dynamics: Fundamentals and Large-Scale Circulation, *Cambridge Univ. Press, Cambridge, UK.*

Vasavada, A. R., and A. P. Showman (2005), Jovian atmospheric dynamics: An update after Galileo and Cassini, *Rep. Prog. Phys., 68*, 1935-1996.

Figure Captions

FIG. 1. Simulation results of one-storm mass forcing at equator after 200 hours. Upper Left: geopotential map; Upper right: zonal-mean zonal wind; Middle left: eddy momentum flux map ($u'v'$); Middle right: zonal-mean eddy momentum flux ($\overline{u'v'}$); Lower left: eddy flux map of vorticity ($\zeta'v'$); Lower right: zonal-mean vorticity flux ($\overline{\zeta'v'}$).

FIG. 2. Simulation results of one-storm mass forcing at 10°N (upper panel) and 30°N (upper panel) after 200 hours. Left: geopotential map; Right: zonal-mean zonal wind.

FIG. 3. Simulation results of multi-storm mass forcing randomly generated from 50°S to 50°N after 2×10^4 hours. Upper left: time evolution of total available potential energy (APE); Upper right: time evolution of total kinetic energy (KE); Lower left: geopotential map; Lower right: zonal-mean zonal wind.

FIG. 4. Simulation results of multi-storm mass forcing after 2×10^4 hours. Upper panel: case with storms randomly generated in the belts only; Lower panel: case with storms concentrated at the equator. Left: geopotential map; Right: zonal-mean zonal wind.

FIG. 5. Simulation results of one-storm vorticity forcing (upper: cyclonic; lower: anticyclonic) at equator after 200 hours. Left: geopotential map; Right: zonal-mean zonal wind.

FIG. 6. Simulation results of one-storm vorticity forcing (upper: cyclonic; lower: anticyclonic) at 30°N after 200 hours. Left: geopotential map; Right: zonal-mean zonal wind.

FIG. 7. Simulation results of two multi-storm vorticity forcing cases after 2×10^4 hours.

Left: geopotential map; Right: zonal-mean zonal wind. The storms in the two cases are both randomly generated from $-50°$S to $50°$N. All the parameters are the same except the random number sequence, but the two cases show very different behaviors.

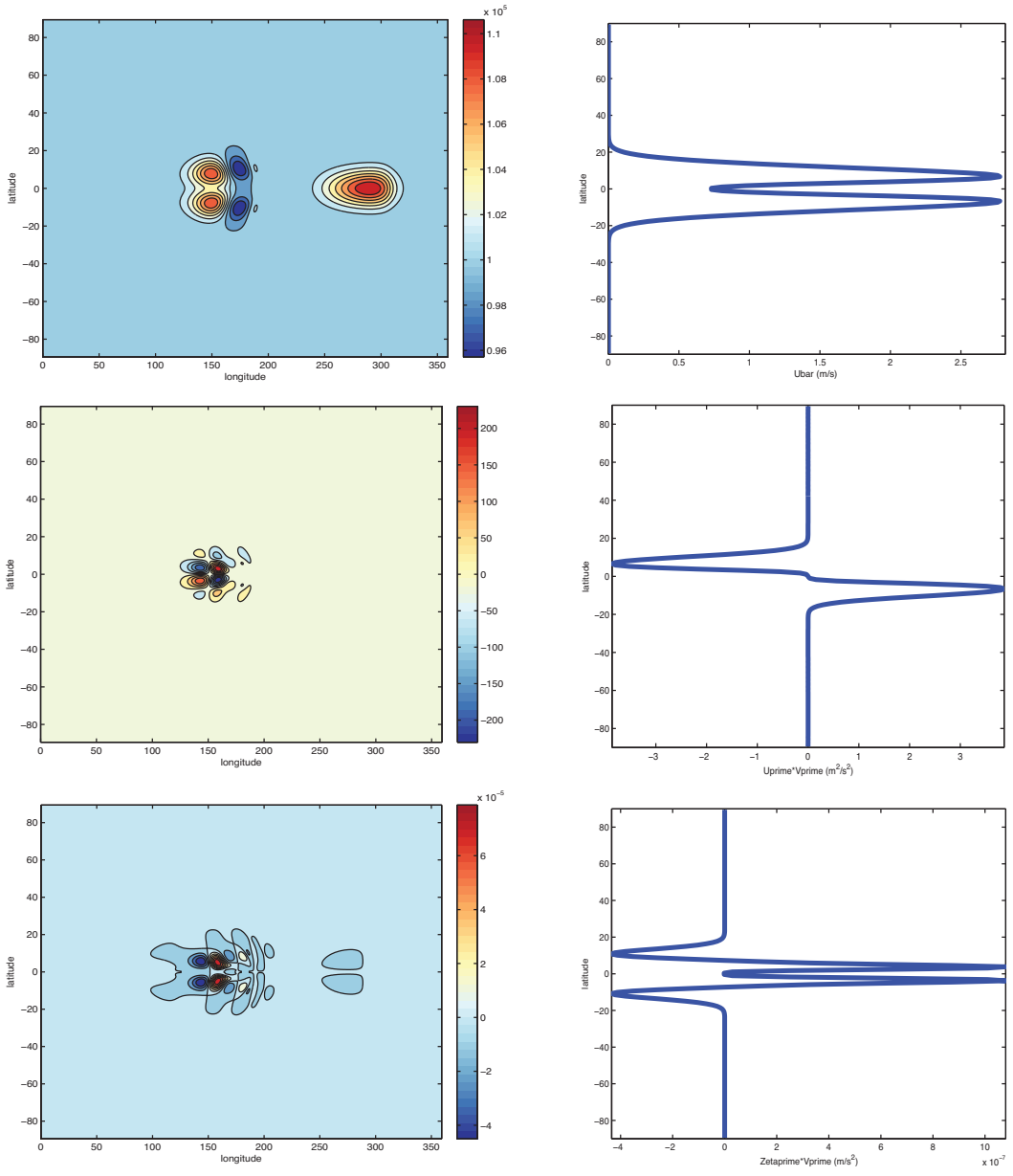
x 10^5
1.1
1.08
1.06
1.04
1.02
1
0.98
0.96
latitude
longitude
Ubar (m/s)
Uprime*Vprime (m^2/s^2)
x 10^-5
6
4
2
0
−2
−4
Zetaprime*Vprime (m/s^2)
x 10^-7

FIG. 1

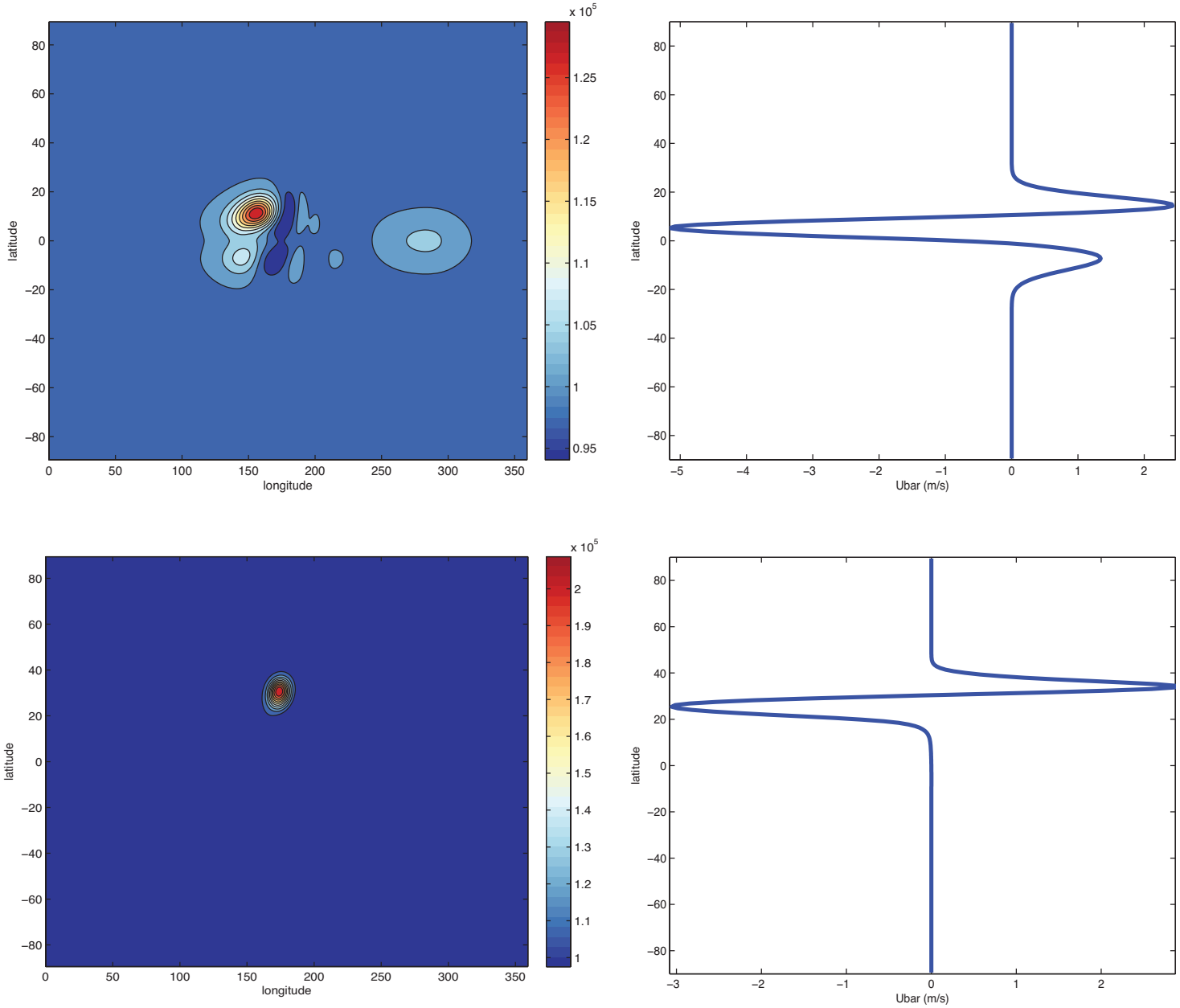
x 10^5
1.25
1.2
1.15
1.1
1.05
1
0.95
latitude
longitude
Ubar (m/s)
x 10^5
2
1.9
1.8
1.7
1.6
1.5
1.4
1.3
1.2
1.1
1

FIG. 2

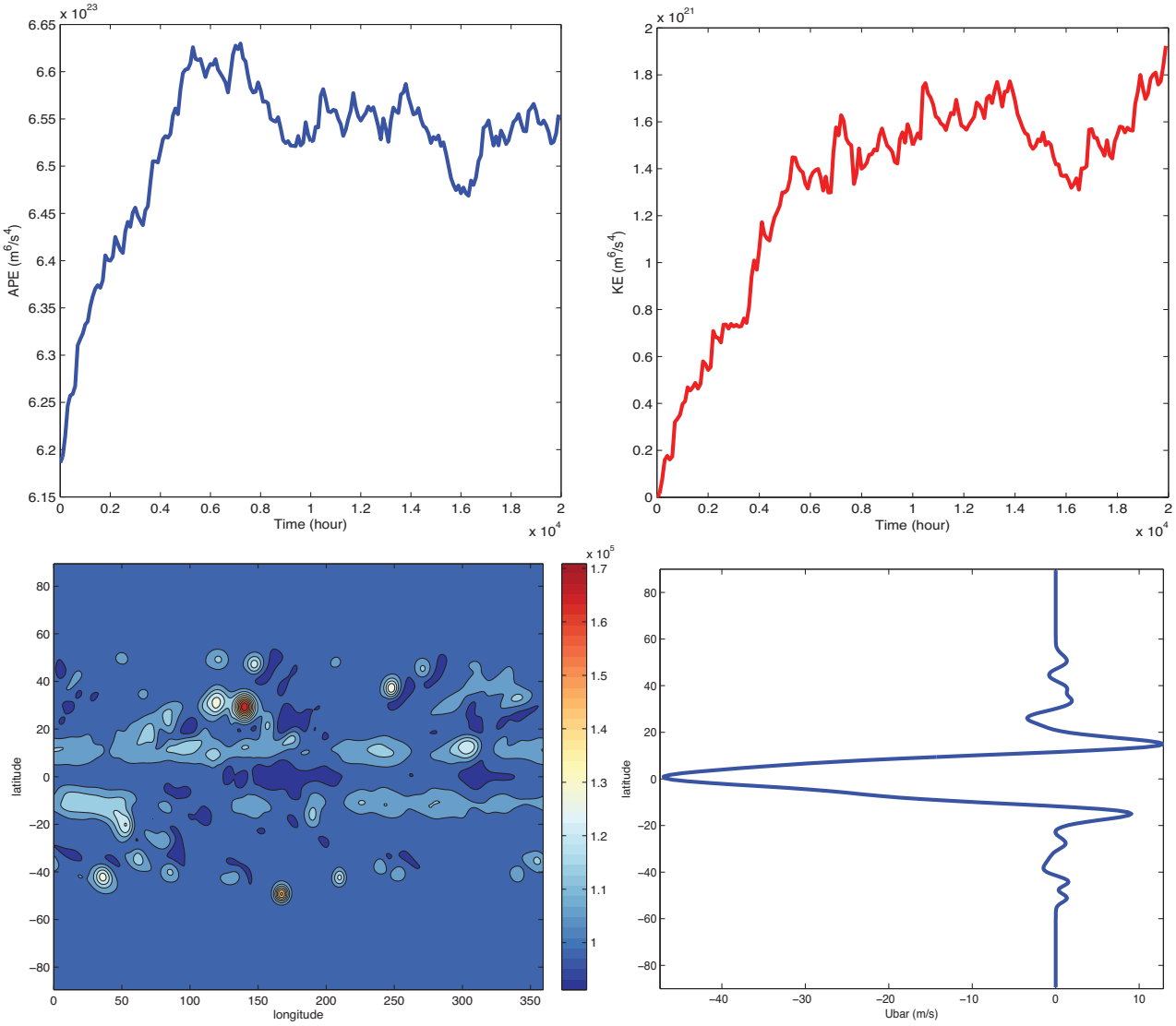
x 10^23
APE (m^6/s^4)
Time (hour)
x 10^4
x 10^21
KE (m^6/s^4)
Time (hour)
x 10^4
x 10^5
latitude
longitude
latitude
Ubar (m/s)

FIG. 3

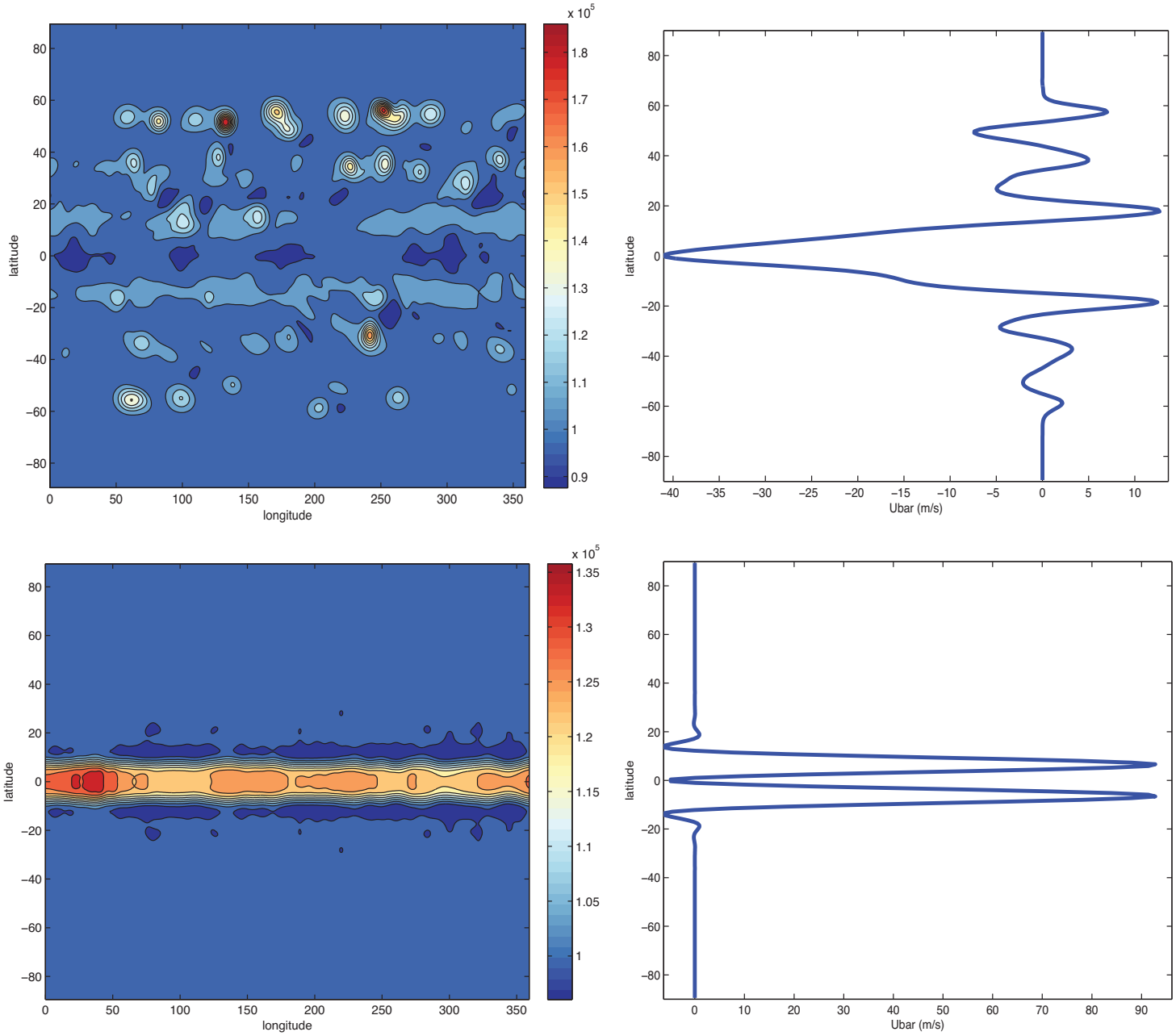
x 10^5
1.8
1.7
1.6
1.5
1.4
1.3
1.2
1.1
1
0.9
latitude
longitude
Ubar (m/s)
x 10^5
1.35
1.3
1.25
1.2
1.15
1.1
1.05
1

FIG. 4

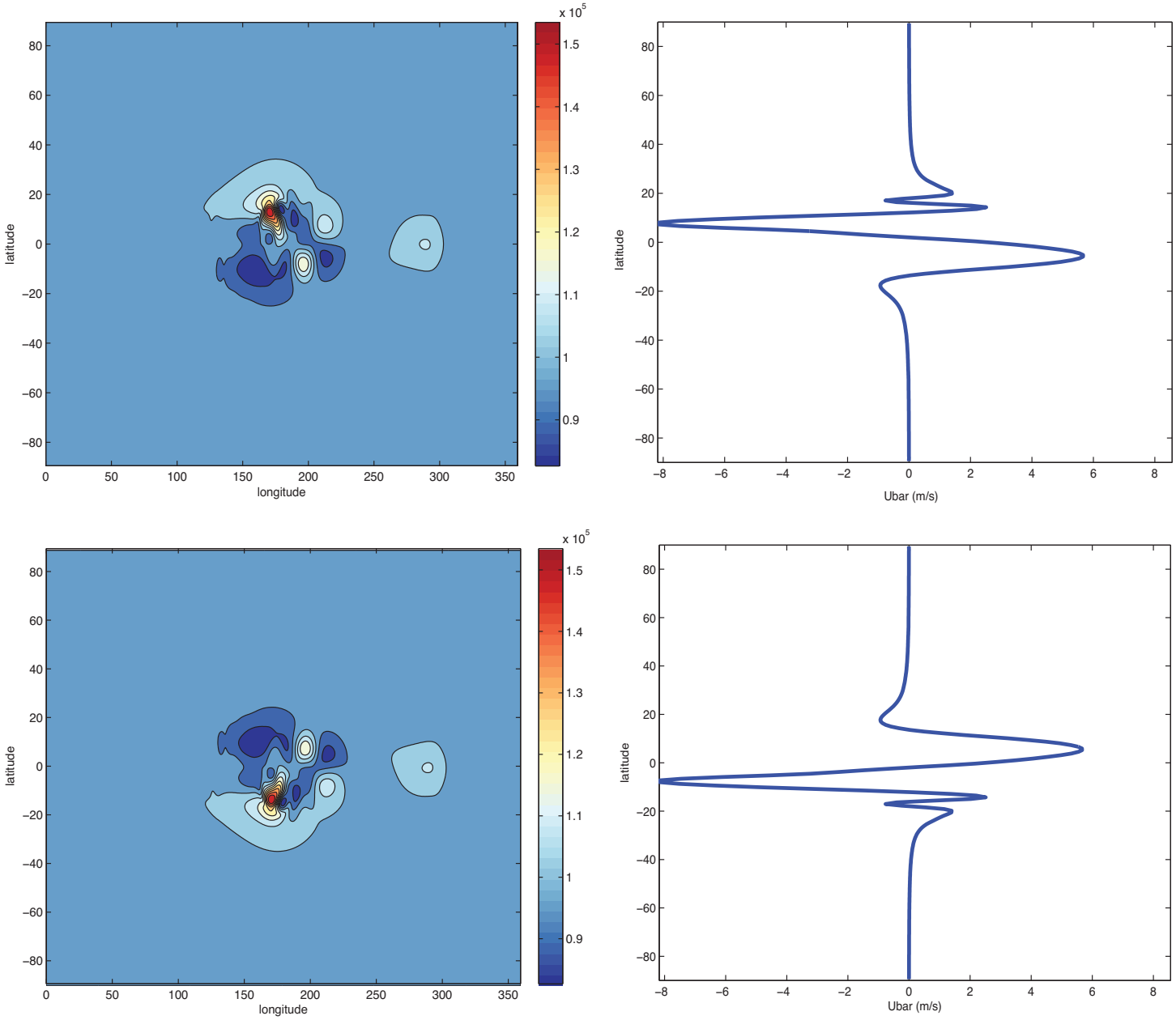
x 10^5
1.5
1.4
1.3
1.2
1.1
1
0.9
latitude
longitude
Ubar (m/s)
80
60
40
20
0
−20
−40
−60
−80
0
50
100
150
200
250
300
350
−8
−6
−4
−2
0
2
4
6
8

FIG. 5

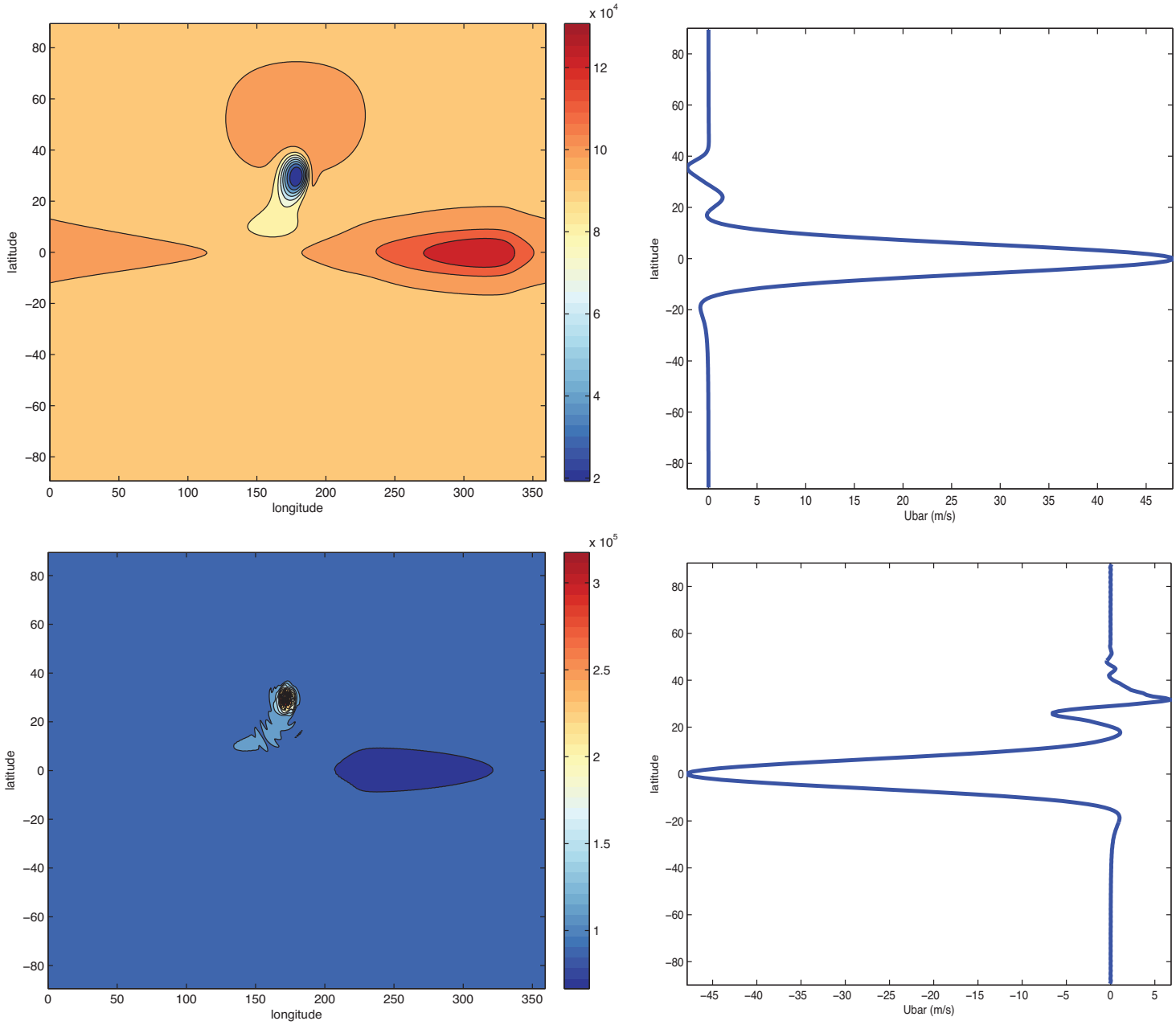

FIG. 6

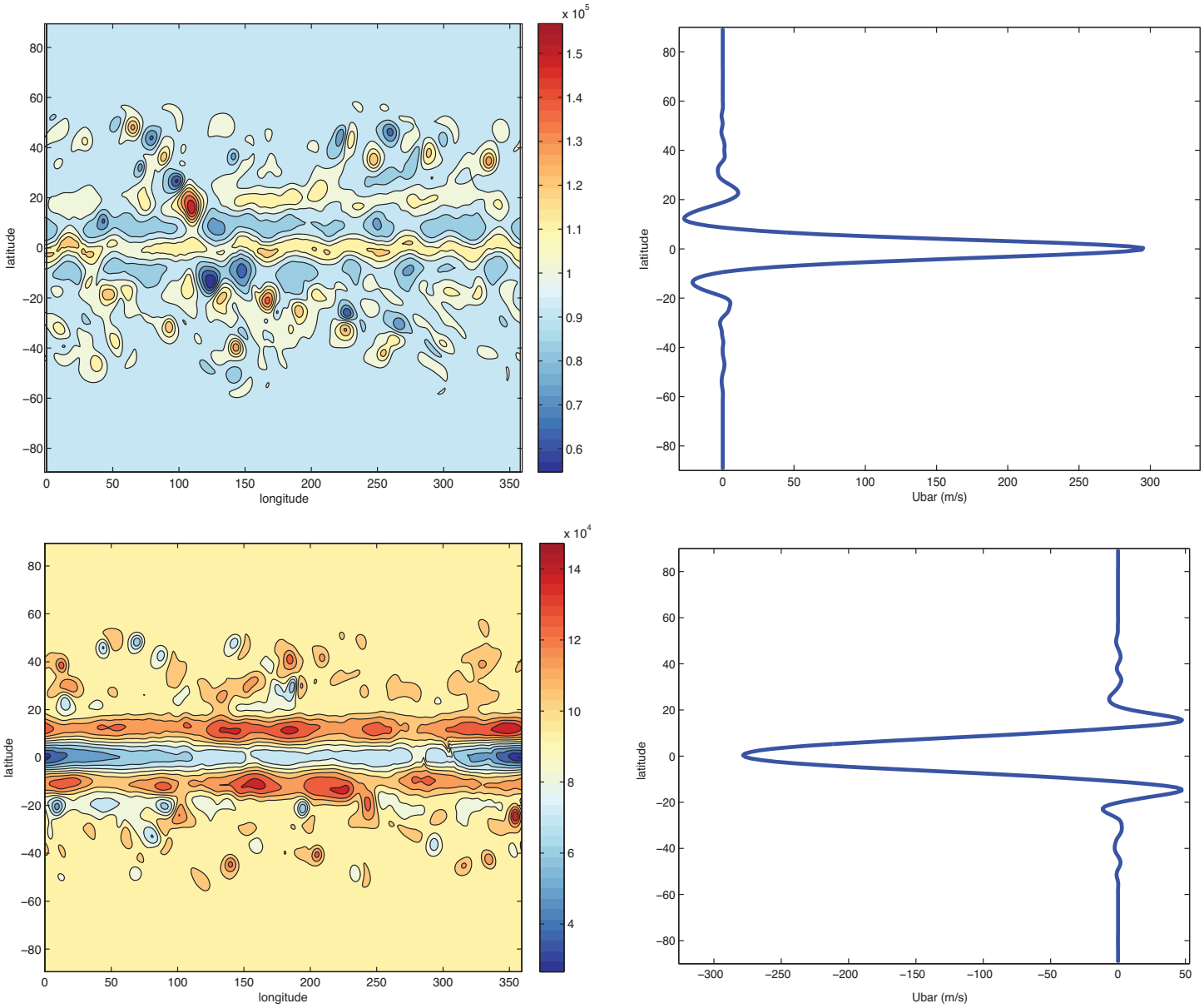
x 10^5
1.5
1.4
1.3
1.2
1.1
1
0.9
0.8
0.7
0.6
latitude
longitude
Ubar (m/s)
x 10^4
14
12
10
8
6
4

FIG. 7